JOURNAL OF AIRCRAFT
Vol. 36, No. 6, November–December 1999

Effects of Wing-Tip Strakes on a Sheared-Tip Wing

Lance W. Traub,* Samuel F. Galls,† and Othon Rediniotis‡
Texas A&M University, College Station, Texas 77843-3141

An experimental investigation was conducted to evaluate the ability of planar and nonplanar wing tip strakes to improve the performance of a 4.18-aspect-ratio rectangular wing with a sheared tip. Strake leading-edge sweep, planform, and anhedral were varied. Force balance measurements, as well as surface-pressure measurement and off-surface smoke flow visualization were undertaken. The results show that planar strakes exhibit a minimal drag penalty compared with the basic wing at low lift coefficients, while recording improvements in efficiency up to 12.8%. Nonplanar strakes can significantly improve the wing efficiency at the expense of a substantial increase in the minimum drag coefficient. Flow visualization showed that the wing-tip vortex system consists of four vortices, two on the strake and two above the wing tip. The forward progression of breakdown of the strake vortices with angle of attack is shown to be slower than would be expected for a delta wing.

Nomenclature

A_s = planform area of both strakes
b_s = semispan of strake
C_A = axial force coefficient
C_D = drag coefficient
$C_{D\min}$ = minimum drag coefficient
C_L = lift coefficient
$C_{L\alpha}$ = lift curve slope
C_m = pitching moment coefficient
C_P = pressure coefficient
e = Oswald efficiency factor
S = wing planform area
s_{tip} = length of sheared tip
x = coordinate along sheared-tip edge
y = spanwise coordinate, perpendicular to sheared wing tip
α = angle of attack
α_{eff} = strake effective angle of attack
α_{ZL} = angle of attack for zero lift
δ = tip strake anhedral angle
Λ_{LE} = tip strake leading-edge sweep angle

Introduction

INVISCID wing efficiency may be improved through planform optimization, spanwise cambering, or attention to wing-tip design. Classical theory shows that for a planar unswept wing of confined span, a wing with elliptical spanwise loading has minimal vortex drag. Cone[1] has shown that, if the wing is not constrained to be planar, numerous nonplanar wing forms (wings with spanwise camber of their lifting lines, end plates, etc.) can improve efficiency beyond the theoretical planar minimum. Wing sweep and crescent planform wings[2] can also accrue drag reduction benefits by the generation of a nonplanar wake through an out-of-plane rotation of the lifting line with incidence. The theoretical magnitudes of the performance enhancements for crescent wings are smaller than those for highly nonplanar tip devices. The sheared tip[3,4] has been extensively studied as a limited implementation of a crescent wing. Generally, experimental studies do not show marked performance improvements for sheared-tip wings.

Received 17 August 1997; revision received 12 April 1999; accepted for publication 4 May 1999.

*Postdoctoral Research Associate, Aerospace Engineering Department. Associate Member AIAA.
†Ph.D. Student, Aerospace Engineering Department. Associate Member AIAA.
‡Assistant Professor, Aerospace Engineering Department.

Several planar and nonplanar wing-tip devices that successfully reduce drag have been tested. Of the nonplanar devices, the winglet[5,6] is probably the most studied. Potential prediction methods[1] show that large drag reductions may be achieved with end plates through the release of vorticity over an appreciable vertical height at the tip, effectively resulting in a reduction in induced downwash, which may be construed as an increase in effective aspect ratio (AR). Experimental studies[7] have generally not realized these performance gains because of the increased profile and interference drag of the end plate. Performance improvements were observed only with the evolution of the end plate into the winglet. Increased performance of winglets is associated with their ability to use the local freestream adjacent to the wing tip to generate a thrust component. Other successful devices are tip sails,[8] which are essentially planar, but use a mechanism similar to winglets to enhance performance. Delta planform tip sails[9,10] are similar to tip sails, but use enforced flow separation to reduce Reynolds number sensitivity and off-design performance. Wing-tip vortex flaps[11] have been shown to use the suction of the wing-tip vortex to generate a thrust component. However, the wings in Ref. 11 were thin and sharp edged and generated no leading-edge thrust. Consequently, it is unlikely that they would be representative of wing forms that would be used in practice.

As mentioned in the preceding text, experimental studies[4] of wings with sheared tips have not shown marked performance improvements for these configurations. Nonetheless, numerous aircraft with sheared tips have recently been designed, thus motivating the present study aimed at enhancing their performance. Consequently, a systematic modification of a blunt-edged sheared tip by means of combination with a wing-tip strake is detailed in this paper. As the test wing was not a flat plate, the results should be of greater utility than those presented in Ref. 11. It is suggested that if the wing-tip vortex forms on the tip strake, then a thrust force may result from this vortex acting on the frontal area of the blunt sheared tip (see Fig. 1). Tip strakes have been tested on various blunt-edged wing planforms.[12] As all the tested configurations[12] had unswept (i.e., parallel to the wing root chord) wing tips, the vortex developed on the strake could not induce any suction on the wing tip or strake that could reduce drag. In the present experimental investigation, planar as well as strakes with anhedral were used. Various tip strake leading-edge sweep angles as well as configurations were tested. The study consisted of force balance, off-surface flow visualization, and pressure measurements.

Equipment and Procedure

The wing was manufactured from aluminium and had a NACA 0011 profile. Sheared tips were made from foam and covered with a plywood skin. The sheared-tips' leading-edge sweep angle was

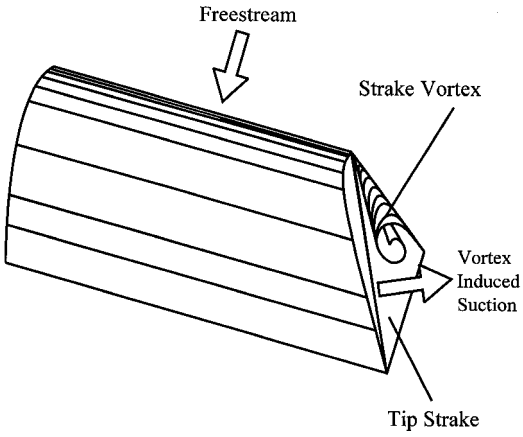

Fig. 1 Vortex formation on sheared wing with a tip strake.

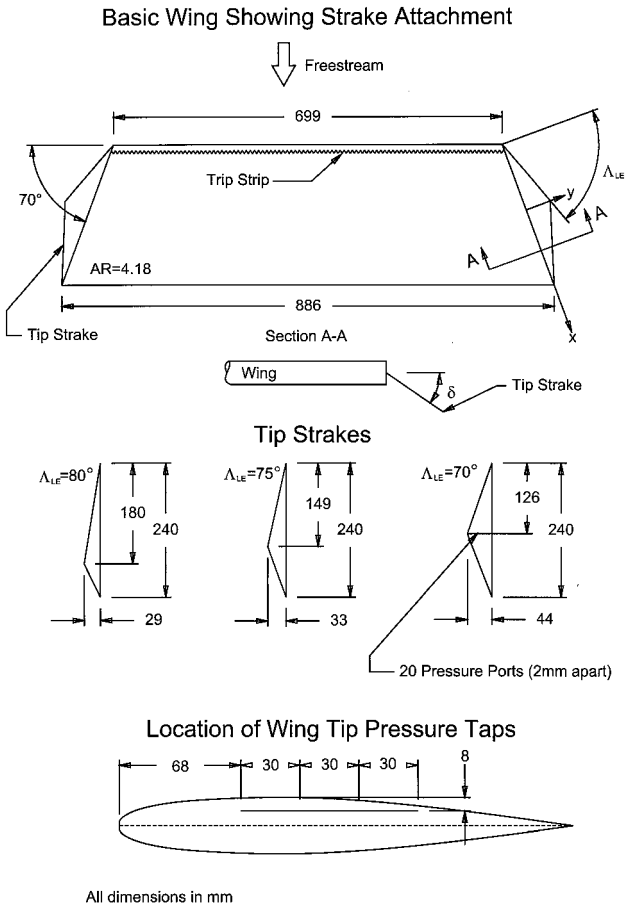

a) Basic wing (AR = 4.18) and planar strakes

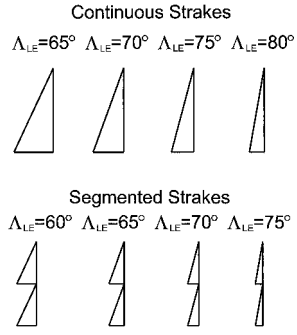

b) δ = 90 deg

Fig. 2 Basic wing and tip strake geometric details.

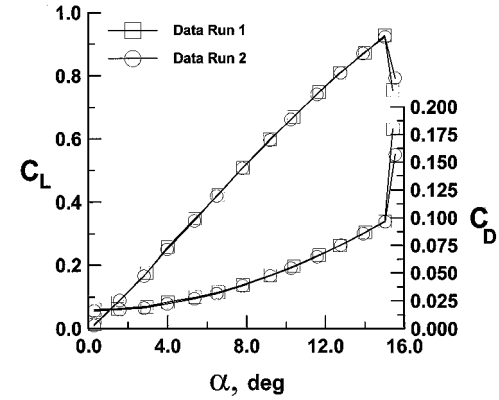

Fig. 3 Repeated data runs for the basic wing.

70 deg. The sheared tips were fixed to the aluminium wing section forming the basic wing. Transition was fixed on the upper and the lower wing surfaces by a trip strip located at 5% of the wing chord. The basic wing's AR was 4.18. The tip strakes were manufactured from 1.3-mm-thick aluminium plate and bent to shape. Details of the models and the strakes are given in Fig. 2.

The tests were undertaken in Texas A&M University's 3 × 4 ft continuous wind tunnel. This tunnel has a turbulence intensity of 0.3% at a freestream velocity of 40 m/s. A six-component Aerolab sting balance was used for force and moment determination. The accuracy of the balance is estimated at 0.6% of full scale for lift, drag, and pitching moment. Balance resolution is better than 2 counts on all channels. Repeatability of the balance for lift, drag, and pitching moment is estimated at $\Delta C_L = 0.0008$, $\Delta C_D = 0.0005$, and $\Delta C_m = 0.0008$. Figure 3 shows two repeated data runs for the basic wing. The model angle of attack can be set to within 0.05 deg. Freestream velocity was measured with a pitot static tube. Differential pressure was measured with an Air Neotronics digital manometer. Force balance data were acquired with a microcomputer equipped with a 16-bit analog-to-digital (A/D) board. The data acquisition code displays graphically real-time lift, drag, and pitching moment. The model was pitched through a set angle of attack ranging from 0 to 15 deg in 1-deg increments. Pitching moment was taken about the wing quarter chord. All forces and moments were nondimensionalized by their respective wing's planform area. At the maximum set angle of attack, blockage was less than 4.5%. Solid and wake blockage were corrected for with the method of Shindo.[13] Corrections for downwash were applied with the method detailed in Ref. 14. The wind-tunnel tests were run at a freestream velocity of 39 m/s yielding a Reynolds number based on the wing's centerline chord of 0.6×10^6. Off-surface flow visualization was conducted at 2.5 m/s, with vaporized kerosene. Surface flow visualization was performed by applying a mixture of kerosene, linseed oil, and titanium dioxide to the surface of the wing.

Results and Discussion

The study involved testing planar and nonplanar tip strakes of various configurations. Initial parameter variation involved changing the strake leading-edge sweep and shape for an anhedral angle of 90 deg. All of these configurations suffered from substantial increases in wing minimum drag, degrading performance well below the basic wing. Salient results for these configurations are, however, included in Tables 1 and 2 to show the trends associated with these configurations. Table 3 contains data for different strake anhedral angles to evaluate the effect of δ on efficiency. For all the tested variations, the wing span was constrained and equal to that of the basic wing. Thus for $\delta < 90$ deg, the tip strakes were progressively cropped to keep the span constant (see Fig. 2a). The lift curve slopes in Tables 1–3 were calculated with the first five data points after the break in the data at $\alpha = 3$ deg; see Fig. 3.

Tables 1 and 2 present a data summary for variations of the strake leading-edge sweep angle for $\delta = 90$ deg. As all the tested wings displayed minimum drag at zero lift, the parabolic drag polar equation

Table 1 Data summary for variation of continuous strake leading-edge sweep angle

Λ_{LE}, deg	$C_{L\alpha}$, per rad	e	$C_{D\min}$	α_{ZL}, deg	δ, deg	AR	S, m^2
Basic wing	3.67	0.86	0.0171	0.05	——	4.18	0.18778
65	3.92	1.09	0.0614	1.44	90	4.18	0.18778
70	3.99	1.09	0.0524	1.15	90	4.18	0.18778
75	3.93	1.01	0.0386	0.99	90	4.18	0.18778
80	3.87	0.96	0.0279	0.60	90	4.18	0.18778

Table 2 Data summary for variation of segmented strake leading-edge sweep angle

Λ_{LE}, deg	$C_{L\alpha}$, per rad	e	$C_{D\min}$	α_{ZL}, deg	δ, deg	AR	S, m^2
Basic wing	3.67	0.86	0.0171	0.05	——	4.18	0.18778
60	3.98	1.02	0.0373	1	90	4.18	0.18778
65	3.91	0.97	0.0325	0.76	90	4.18	0.18778
70	3.88	0.93	0.0263	0.69	90	4.18	0.18778
75	3.84	0.89	0.0222	0.55	90	4.18	0.18778

Table 3 Data summary for variation of continuous strake anhedral angle

Λ_{LE}, deg	$C_{L\alpha}$, per rad	e	$C_{D\min}$	α_{ZL}, deg	δ, deg	AR	S, m^2
Basic wing	3.67	0.86	0.0171	0.05	——	4.18	0.18778
70	3.77	1.06	0.0411	1.35	75	4.08	0.19240
70	3.70	0.98	0.0289	1.04	60	4.03	0.19479
70	3.65	0.94	0.0237	0.74	45	4.00	0.19625
70	3.72	0.96	0.0173	0.30	0	3.98	0.19724
75	3.71	0.97	0.0351	1.01	75	4.11	0.19100
75	3.67	0.93	0.0253	0.90	60	4.07	0.19287
75	3.59	0.95	0.0217	0.69	45	4.04	0.19431
75	3.70	0.97	0.0167	0.38	0	4.02	0.19527
80	3.66	0.94	0.0164	0.26	0	4.05	0.19383

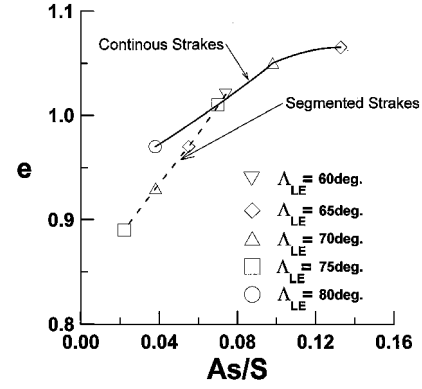

Fig. 4 Effect of A_s/S on wing efficiency factor for continuous and segmented strakes; δ = 90 deg.

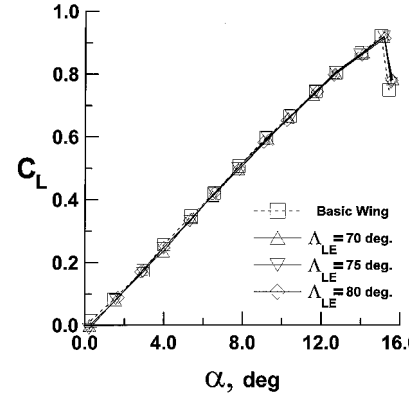

Fig. 5 Effect of strake leading-edge sweep angle on lift coefficient, δ = 0 deg.

was used to calculate e, with the slope of the linearized drag polar. Sweep is seen to have a moderate effect on wing lift curve slope; however, all variations show increased $C_{L\alpha}$ over the basic wing. The improvement in the lift curve slope is a consequence of reduced downwash as a result of the nonplanar wake (i.e., the strake effectively induces an upwash over the wing or, alternatively, provides an obstacle to the wing-tip flow, thereby reducing downwash). Wing efficiency is seen to increase dramatically over the basic wing, with efficiencies above the theoretical planar minimum ($e = 1$) being recorded. Increasing the strake sweep is seen to reduce e. The increases in efficiency are due to wake nonplanarity, as well as to the inclined strakes' generating thrust. All the performance benefits are, however, offset by the substantial increase in $C_{D\min}$, which essentially mitigates any potential performance improvements. At $\alpha = 0$ deg, the strakes result in the wing's generating negative lift because of vortical formation on the lower surface, causing these wings to have α_{ZL} shifted positive.

In an attempt to reduce the substantial minimum drag of the tip devices, they were segmented as shown in Fig. 2b. Segmenting[15] has been used successfully on vortex flaps to improve the flaps' ability to retain the leading-edge vortex. Segmenting is seen to reduce the wing efficiency; however, it also results in a reduction of $C_{D\min}$ of approximately 50% for some configurations (Table 2).

To determine how effectively the tip devices use their wetted area, Fig. 4 presents the wing efficiency factor as a function of the strake area divided by the wing area for both the continuous and the segmented strakes. It may be seen that increasing strake area increases wing efficiency linearly. For the continuous strakes, however, the benefit of increasing A_s/S beyond approximately 0.1 is seen to be reduced. For a high strake sweep (low A_s/S) the segmented strakes have lower efficiency than the continuous strakes for the same wetted area. However, note that the segmented strakes appear to be more sensitive to area changes, i.e., $\partial e/(\partial A_s/S)$ is larger.

Decreasing the strake's anhedral (Table 3) results in a reduction in wing $C_{L\alpha}$ for all tip strakes. For $\delta = 0$ deg, however, $C_{L\alpha}$ appears insensitive to variations of strake sweep angle (Λ_{LE}). This suggests that lift enhancement effects consist of two components: one that is due to nonplanar effects, resulting in a reduction in $C_{L\alpha}$ with decreasing anhedral, and one that is due to vortex lift on the strake, which increases with decreasing anhedral. For the planar cases and the basic wing, the wing lift curve slope was estimated with a vortex lattice code,[16] with 10 chordwise panels and 20 spanwise panels. The panel method gives $C_{L\alpha} = 3.7, 3.72, 3.74$, and 3.73/rad for the basic wing, $\Lambda_{LE} = 70, 75$, and 80 deg respectively. These values compare well with those determined experimentally (Table 3, $\delta = 0$ deg). The panel method does, however, show a weaker dependence on the strake leading-edge sweep angle than the experimental results suggest.

For strake sweeps of 70 and 75 deg, decreasing the anhedral angle generally reduces the wing efficiency (Table 3). Decreasing the wing's anhedral also reduces the minimum drag coefficient penalty substantially.

The three presented cases in Table 3 with $\delta = 0$ deg have minimum drag coefficient values, $C_{D\min}$, comparable with the basic wing and higher efficiencies. In the following discussion, the performance characteristics of these configurations are detailed.

Figures 5 and 6 present lift curves and drag polars, respectively, for various sweep angles with $\delta = 0$ deg. Despite the moderate reduction in AR for the wing with tip strakes, Fig. 5 shows that all the configurations have a performance similar to that of the basic wing. Figure 6a shows that for $C_L < 0.3$, the basic wing has a small drag advantage over the wing with strakes. However, for $C_L \geq 0.6$, all the tip strake variations show a drag reduction compared with that of the basic wing. Figure 6b shows the variation of C_D with C_L^2: the linearized drag polar. The decreased slope of the polar for the tip strake configurations compared with the basic wing is a clear manifestation of increased aerodynamic efficiency.

Figure 7 shows the L/D ratio as a function of C_L for $\delta = 0$ deg. The results show that the wings with strakes (specifically $\Lambda_{LE} =$ 75 deg) improve the lift-to-drag ratio over the basic wing for

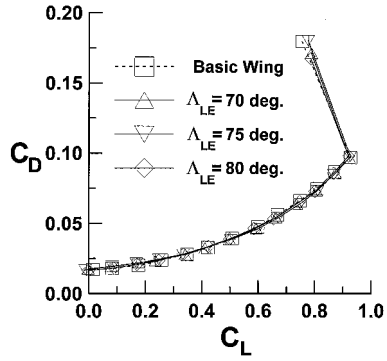

a) Drag polar

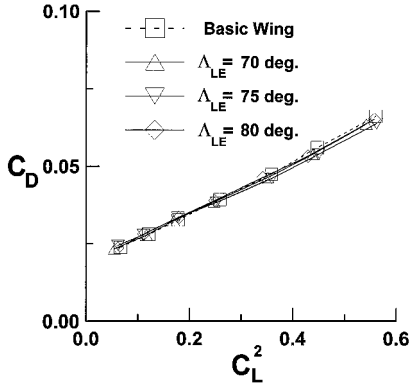

b) Linearized drag polar

Fig. 6 Effect of strake leading-edge sweep angle on drag coefficient, $\delta = 0$ deg.

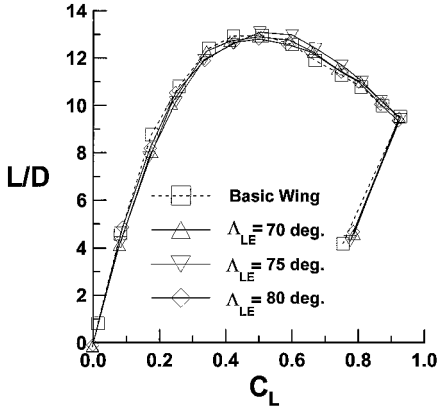

Fig. 7 Effect of strake leading-edge sweep angle on *L/D* ratio, $\delta = 0$ deg.

$C_L > 0.50$. To avoid any performance degradation, the tip strakes could be designed so as to be retractable and deployed in a flight regime only in which they augment performance. As shown in Table 3, all three of the planar wings with strakes improve wing efficiency over the basic wing by 9.3–12.8%. These substantial improvements are not obvious from Fig. 7 [as for a symmetrical profile, $(L/D)_{\max} = \frac{1}{2}(\pi \mathrm{AR}e/C_{D\min})^{1/2}$]. This increase in efficiency is primarily due to the reduced AR of the wings with strakes as $e = (\partial C_L^2/\partial C_D)/\mathrm{AR}\pi$ and is reflected in their ability to improve performance moderately over the basic wing, despite the lower AR.

Axial force variation (or leading-edge suction, as the wing is planar, and thus experiences no camber thrust) is shown in Fig. 8. The values shown have their minimum drag removed. The figure shows that the wing with strakes does generate a moderate increase in axial force over the basic wing for $C_L > 0.6$. As the strake wings do not benefit from a lift increment over the basic wing for this α range (Fig. 5), the increase in axial force must come from a thrust increase as a consequence of the strake vortex acting on the forward-sloping

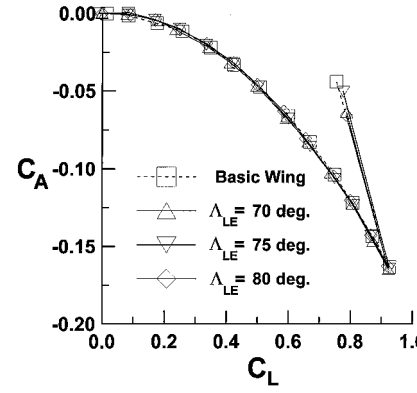

Fig. 8 Effect of strake leading-edge sweep angle on axial force coefficient, $\delta = 0$ deg.

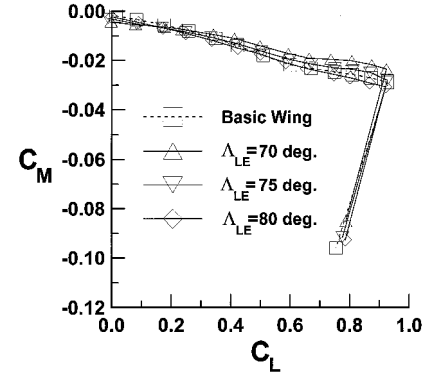

Fig. 9 Effect of strake leading-edge sweep angle on pitching moment coefficient, $\delta = 0$ deg.

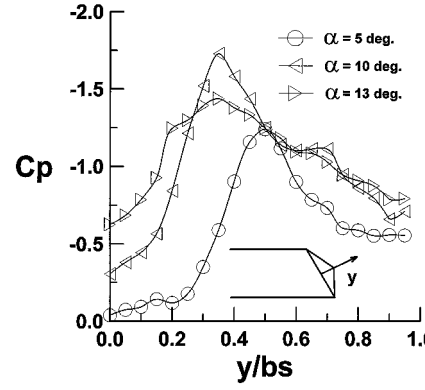

Fig. 10 Effect of α on spanwise pressure distribution over tip strake, $\Lambda_{LE} = 70$ deg and $\delta = 0$ deg.

sheared-tip edge. As shown below, the strake vortex is capable of generating significant suction.

Pitching moment as a function of lift coefficient is presented in Fig. 9. All the plots show an increase in nose-down pitching moment compared with a symmetrical wing with an unswept quarter chord, which is due to the aft shift of the center of area with the sheared-tip attachment. Addition of the strakes to the basic wing results in a lessened nose-down moment, which is due to a forward shift of the tip's center of area.

To determine the nature of the flow over the strakes, the planar strake with a sweep of 70 deg was pressure tapped, with a row of 20 spanwise tappings spaced 2 mm apart, as shown in Fig. 2a. Pressures were recorded for $\alpha = 5$, 10, and 13 deg (Fig. 10). As may be seen, a suction peak associated with vortical flow is clearly evident. The vortex is seen initially to migrate inboard with increasing α. The magnitude of the suction peaks is also seen to be substantial, e.g.,

for $\alpha = 5$ deg, the minimum pressure recorded was $C_P = -1.24$. For a sharp-edged 60-deg delta, Rinoie and Stollery[17] recorded the minimum pressure under the vortex at a similar chordwise location, as -0.82 at $\alpha = 6.1$ deg. Although, because of differing sweeps, one cannot directly compare the data, the comparison does suggest that the tip strake vortices may generate a minimum pressure lower than their geometric α would suggest. Assuming conical flow, C_P is a linear function of angle of attack. This would imply an effective α for the strake of approximately 9 deg (i.e., $\alpha_{\text{eff}} = -1.24 \times 5/(-0.82 \times 5/6.1)$. This value compares well with the measured flow angularity adjacent to the wing tip of a rectangular blunt-edged wing at a geometric α of 5 deg (Ref. 18). This suggests that the tip strake is effectively embedded in the wing-tip flow and thus experiences flow angularities larger than the geometric α, thereby enhancing its effectiveness. The pressure distribution at $\alpha = 13$ deg shows that vortex breakdown has occurred, with a relatively flat pressure distribution present. As shown subsequently, off-surface flow visualization shows clear vortex breakdown at this location and angle of attack.

Figure 11 shows the measured pressure distribution at four tappings (see Fig. 2) along the side edge of the sheared tip. The data show that the effect of the strake vortex is to increase greatly the suction along the side edge of the wing and thus generate a thrust component. The high suction peak for the basic wing at the most forward pressure tapping and $\alpha = 5$ deg is most likely associated with the presence of a secondary vortex along the side edge of the tip. This vortex moves away from that tap with increasing α, leading to a reduction in the measured suction.

Figures 12 and 13 show off-surface smoke flow visualization for the basic wing and for the wing with the $\Lambda_{\text{LE}} = 70$ deg at $\delta = 0$ deg. Figure 14a shows the arrangement of the wing and the tip strakes used for each photograph in Figs. 12 and 13. Figure 14b presents a summary of the flowfield structures observed over the wing with tip strakes and Fig. 14c over the basic wing. Figures 12a–12c show that the basic wing's vortex system consists of two vortices, an inner or primary vortex, and a secondary vortex of opposite rotation formed adjacent to the leading edge. The secondary vortex forms as a result of separation of the boundary-layer flow passing laterally spanwise under the primary vortex, as it encounters the adverse pressure gradient associated with passage beyond the core of the vortex. Note that for $\alpha = 9$ and 14 deg, breakdown of the primary vortex is visible at the wing's trailing edge. Unlike delta wings, however, the breakdown shows no clear movement upstream with increasing angle of attack. It may be seen that the primary and the secondary vortices are formed at the upper surface of the wing leading edge. For a square-edged blunt wing[19] these vortices form on the blunt side edge, and roll over onto the upper surface.

Figures 13a–13c show the flowfield over the $\Lambda_{\text{LE}} = 70$ deg strake. Although not clear in the figures, video footage taken during the tests showed clearly that the wing-tip flowfield consists of four vortices, two on the strake and two above the wing tip. At $\alpha = 9$ and 14 deg, the primary strake vortex is seen to burst, with the burst position moving upstream with increasing incidence, as would be expected for a conventional delta wing. Note that for $\alpha = 14$ deg, the breakdown location is ahead of the location of the pressure taps, as was surmized above.

The $\Lambda_{\text{LE}} = 75$ and 80 deg cases (not shown) revealed a flowfield essentially similar to $\Lambda_{\text{LE}} = 70$ deg (Figs. 13a–13c). However,

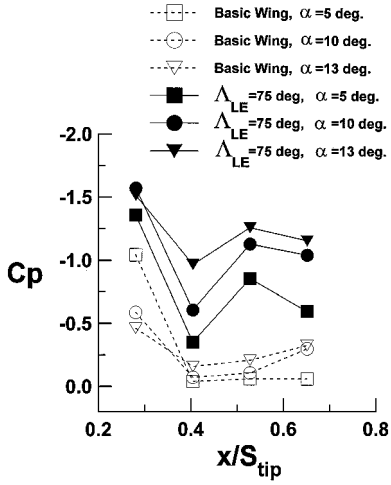

Fig. 11 Effect of α on chordwise pressure distribution over sheared tip of basic wing and wing with strake, $\Lambda_{\text{LE}} = 70$ deg and $\delta = 0$ deg.

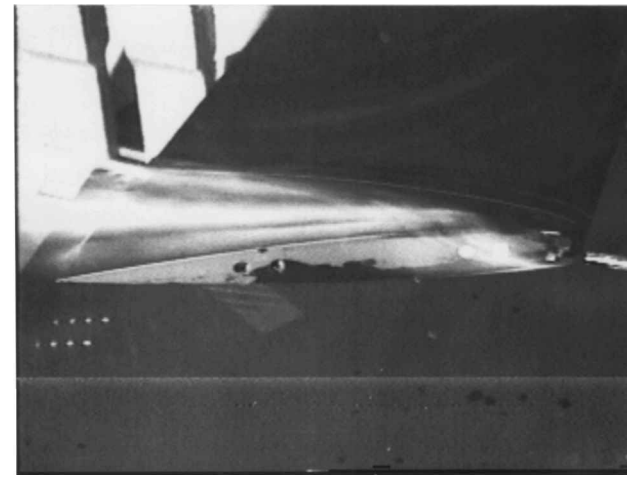

a) α = 5 deg

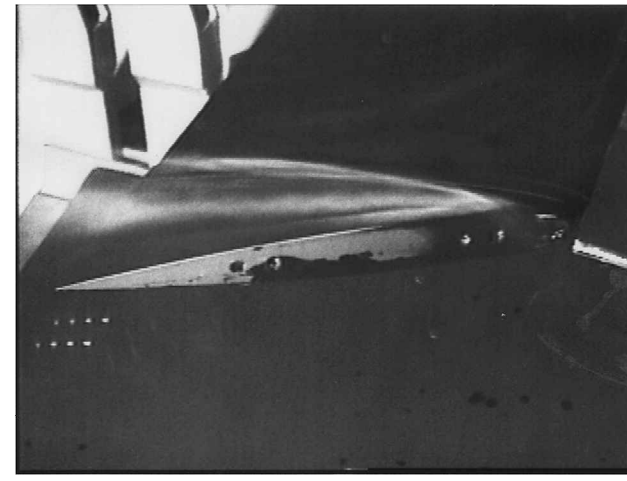

b) α = 10 deg

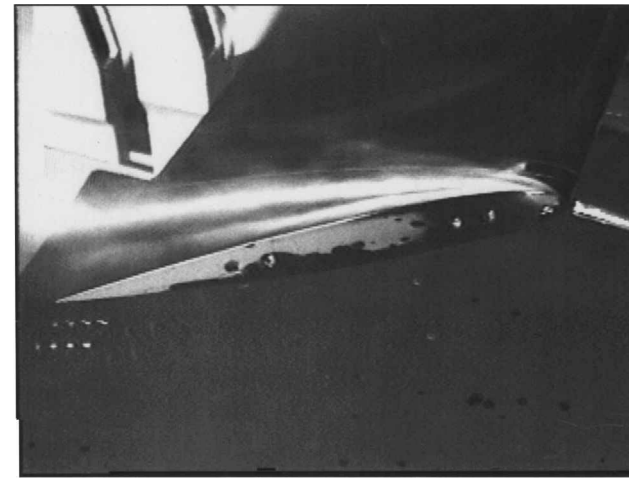

c) α = 13 deg

Fig. 12 Smoke flow visualization over basic wing.

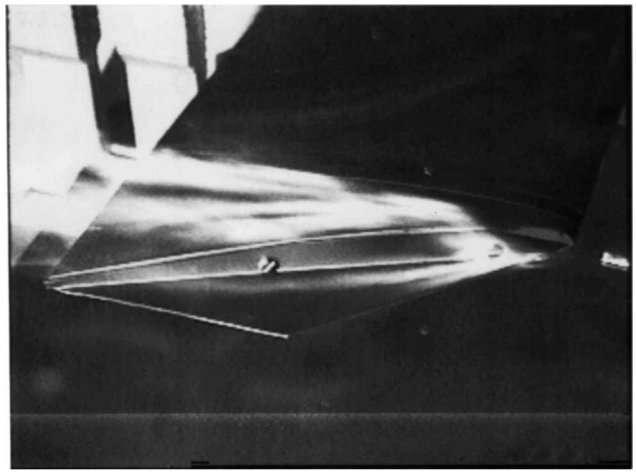

a) α = 5 deg

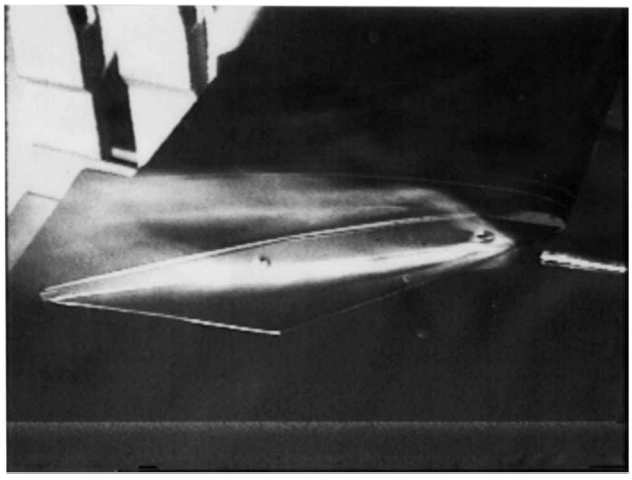

b) α = 10 deg

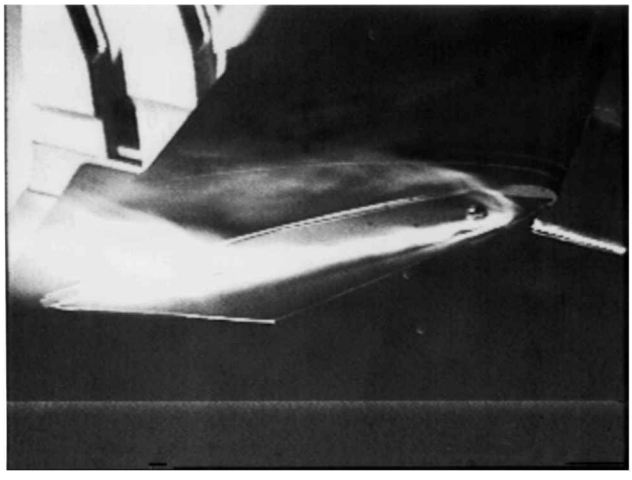

c) α = 13 deg

Fig. 13 Smoke flow visualization over Λ_{LE} = 70-deg tip strake and δ = 0 deg.

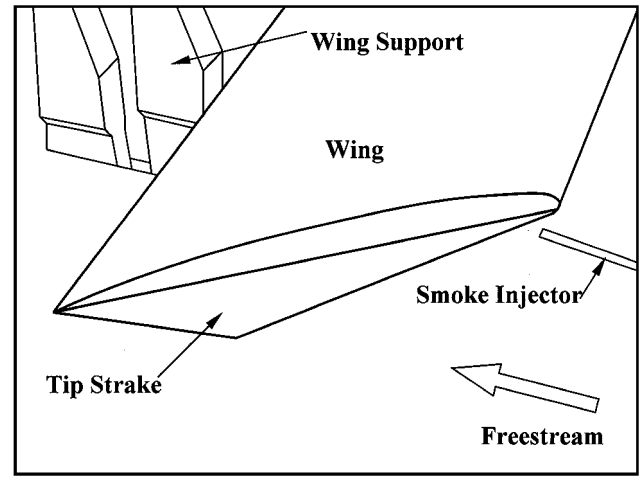

a) Arrangement used in Figs. 12 and 13

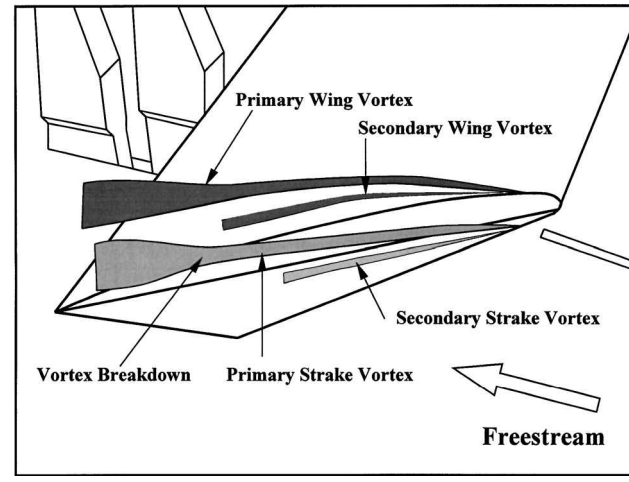

b) Observed flow features over the strake wing

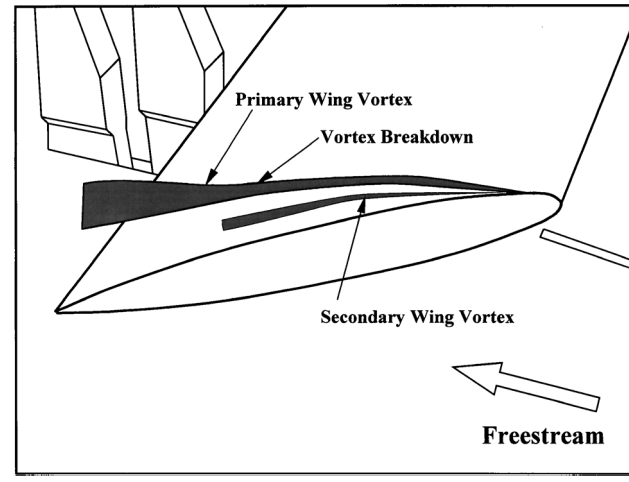

c) Observed flow features over the basic wing

Fig. 14 Summary of the arrangement and flow observations of the wing and the strakes.

the differing leading-edge sweep angles of these strakes seemed to have no apparent effect on the vortex flowfield in terms of breakdown characteristics. This result is unusual and not observed in breakdown data for delta wings. For all cases (Λ_{LE} = 70, 75, and 80 deg), the rate of progression of the breakdown location is slower than that for pure deltas where for $\Delta\alpha$ = 10 deg, breakdown may progress 0.6 of the wing root chord.[20] The flow visualization results certainly suggest that the resulting wing-tip flowfield is complicated, and generally the interaction of the wing tip and the strake flows is such that a flowfield more favorable to delay vortex breakdown results. It is suggested that the sheared tip in concert with the strake may essentially form a converging channel on the upper strake surface, thus lessening the adverse pressure gradient normally associated with enforcement of the Kutta condition and its associated pressure recovery. This would explain why breakdown, although visible near the trailing edge at low α, progresses forward slowly

with increasing incidence as the vortex circulation increases. For all the tested cases, breakdown appears to be of the bubble type, as opposed to the more common spiral type usually seen on delta wings.

It is noteworthy that for all strake sweep angles and tested angles of attack, the strake vortex generally remains above the strake and does not roll over onto the upper wing surface, enhancing its effectiveness by constraining it against the sheared-tip side edge. Leading-edge vortex flaps[15] are prone to "loosing" the leading-edge vortex at high α, as the vortices expand and migrate inboard. It is probable that the sidewash from the primary wing vortex, as well as the larger sweep angle of the sheared-tip side edge as opposed to the strake leading edge, helps to confine the strake vortex above the strake. Leading-edge vortex flaps usually have a lesser or an equal leading edge sweep to that of their flap hinge line.

Figure 15 shows the surface flow visualizations for the basic wing and that with the $\Lambda_{LE} = 75$ deg tip strake. The skin friction patterns shown in Fig. 15 indicate that the trip strip did indeed "trip" the boundary layer with a small localized separation present just in front of the strip. A comparison of Figs. 15a and 15b shows that the surface flow is not particularly sensitive to the small change in α presented, although the tip vortex increases in size. Despite the continually decreasing local chord and hence Reynolds number of the sheared-tip section, the tip region does not show any obvious Reynolds number effects. This is because the primary wing tip vortex dominates the tip flowfield in a manner analogous to that of the vortices over a delta wing. The vortical flow thus eliminates any localized separation that may be precipitated by the local decrease of the Reynolds number. The skin friction patterns in Figs. 15a and 15b show a secondary separation line adjacent to the tip, which agrees with the observed secondary separation vortex seen in the off-surface flow visualization.

The addition of the tip strake (see Figs. 15c and 15d) does not inhibit the formation of a wing-tip vortex over the sheared tip. The skin friction patterns indicate the formation of a vortex on the strake, which is also associated with a secondary separation line. A comparison of the flow patterns in Figs. 15b–15d show strong interaction between the strake and wing vortices, with strake-induced sidewash displacing the wing vortex inboard. The wingtip/strake flowfield shows sensitivity to α (compare Figs. 15c and 15d) with an increase in incidence from 5 to 10 deg, displacing the wing tip vortex further inboard, which is most marked near the trailing edge. This may be a result of the strake vortex locally rolling over onto the upper wing surface near the trailing-edge location.

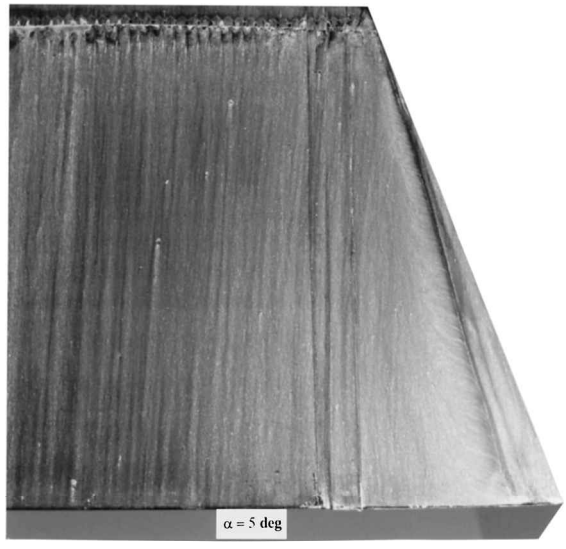

a) Basic wing, α = 5 deg

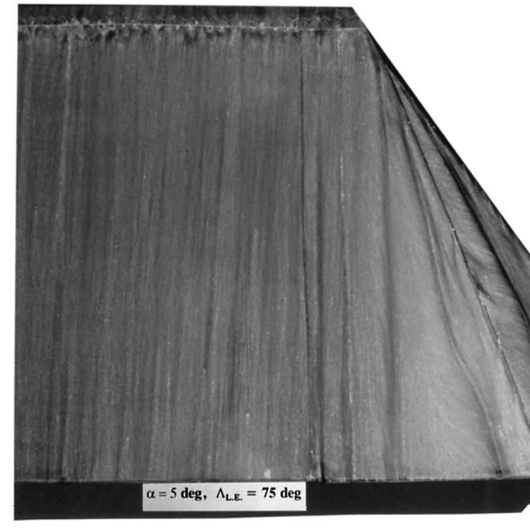

c) Planar tip strakes, α = 5 deg and Λ_{LE} = 75 deg

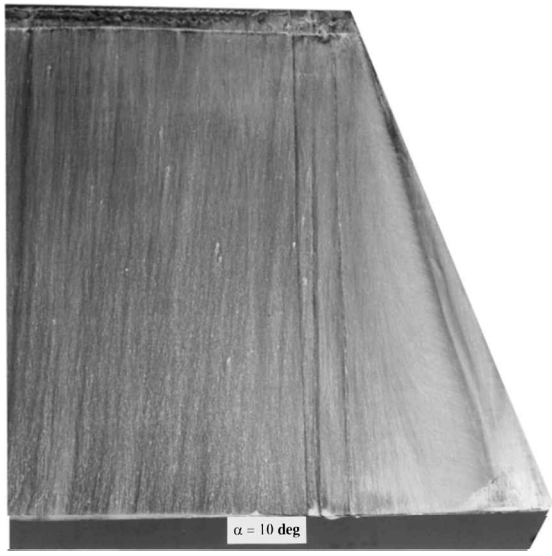

b) Basic wing, α = 10 deg

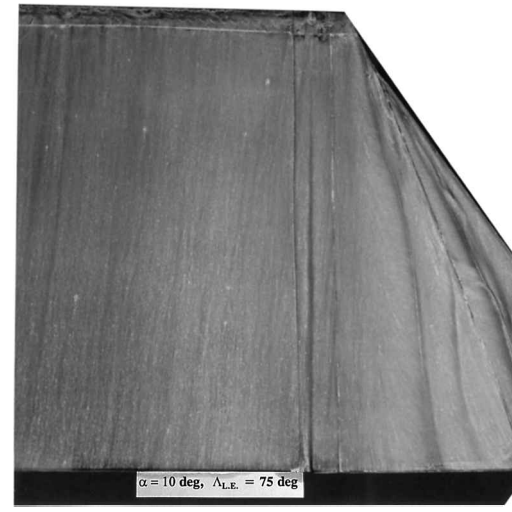

d) Planar tip strakes, α = 10 deg and Λ_{LE} = 75 deg

Fig. 15 Surface flow visualization.

It must be noted that the present study was undertaken at a low Reynolds number; thus the results may not be representative of those at higher Reynolds numbers. However, the strakes are thin and highly swept, thereby enforcing flow separation and thus reducing their sensitivity to Reynolds number effects. Consequently the observed trends (if not magnitudes) should still be applicable at higher Reynolds numbers.

Conclusions

An experimental study was undertaken to evaluate the ability of planar and nonplanar wing-tip strakes to improve the performance of a 4.18 aspect ratio rectangular wing with a sheared tip. In the investigation, strake leading-edge sweep, planform, and anhedral were varied.

From the experimental results the following conclusions are drawn:

Planar strakes show a minimal drag penalty compared with that of the basic wing at low lift coefficients, while recording improvements in efficiency up to 12.8%. Lifting performance is similar to the basic sheared wing. Surface-pressure measurements showed that the strake vortex is capable of generating substantial suction levels. Flow visualization showed that the wing-tip vortex system consists of four vortices, two on the strake and two above the wing tip. The breakdown location of the strake vortices is shown to have a slower forward progression rate, with increasing incidence, than would be expected for a delta wing.

Nonplanar strakes can significantly improve the wing efficiency; however, this is at the expense of a substantial increase in the minimum drag coefficient. The wing zero lift angle of attack shifts progressively more positive as the strake anhedral increases. For the nonplanar strakes, increasing their leading-edge sweep reduces the wing efficiency, with a concomitant decrease in the minimum drag coefficient. Segmenting the strakes decreases efficiency, but does reduce the drag penalty.

Acknowledgments

The authors thank Conrad Wilson for the manufacture of the test wing. Leland Carlson's helpful suggestions are also appreciated.

References

[1]Cone, C. D., Jr., "The Theory of Induced Lift and Minimum Induced Drag of Nonplanar Lifting Systems," NASA TR-R-139, 1962.

[2]van Dam, C. P., "Induced Drag Characteristics of Crescent-Moon-Shaped Wings," *Journal of Aircraft*, Vol. 24, No. 2, 1987, pp. 115–119.

[3]Vijgen, P. M. H. W., van Dam, C. P., and Holmes, B. J., "Sheared Wing Tip Aerodynamics: Wind Tunnel and Computational Investigation," *Journal of Aircraft*, Vol. 26, No. 3, 1989, pp. 207–213.

[4]Naik, D. A., and Ostowari, C., "Effects of Nonplanar Outboard Wing Forms on a Wing," *Journal of Aircraft*, Vol. 27, No. 2, 1990, pp. 117–122.

[5]Heyson, H. H., Riebe, G. D., and Fulton, C. L., "Theoretical Parametric Study of the Relative Advantages of Winglets and Wing Tip Extensions," NASA TP 1020, Sept. 1977.

[6]Asai, K., "Theoretical Considerations in the Aerodynamic Effectiveness of Winglets," *Journal of Aircraft*, Vol. 22, No. 7, 1985, pp. 635–637.

[7]Hoerner, S. F., *Fluid Dynamic Lift*, published by the author, Brick Town, NJ, 1975, Chap. 3, pp. 9–12.

[8]Spillman, J. J., "Wing Tip Sails; Progress to Date and Future Developments," *Aeronautical Journal*, Vol. 91, No. 12, 1987, pp. 445–453.

[9]Traub, L. W., "Aerodynamic Effects of Delta Planform Tip Sails on Wing Performance," *Journal of Aircraft*, Vol. 31, No. 5, 1994, pp. 1156–1159.

[10]Traub, L. W., "Effects of Delta Planform Tip Sail Incidence and Arrangement on Wing Performance," *Journal of Aircraft*, Vol. 32, No. 5, 1995, pp. 1160–1162.

[11]Traub, L. W., "Effects of Wing Tip Vortex Flaps," *Journal of Aircraft*, Vol. 30, No. 4, 1993, pp. 557–560.

[12]Ma, E. C., "Effect of Wing Tip Strakes on Wing Lift-Drag Ratio," *Journal of Aircraft*, Vol. 26, No. 5, 1989, pp. 410–416.

[13]Shindo, S., "Simplified Tunnel Correction Method," *Journal of Aircraft*, Vol. 32, No. 1, 1995, pp. 210–213.

[14]Pope, A., and Rae, W. H., *Low Speed Wind Tunnel Testing*, Wiley, New York, 1984, pp. 199–208, 362–424.

[15]Rao, D. M., "An Exploratory Study of Area Efficient Vortex Flap Concepts," *Journal of Aircraft*, Vol. 20, No. 12, 1983, pp. 1062–1067.

[16]Lamar, J. E., and Gloss, B. B., "Subsonic Aerodynamic Characteristics of Interactive Lifting Surface with Separated Flow Around Sharp Edges Predicted by a Vortex Lattice Method," NASA TN-D 7921, Sept. 1975.

[17]Rinoie, K., and Stollery, J. L., "Experimental Studies of Vortex Flaps and Vortex Plates; Part 2. 1.15 m Span 60 Delta Wing," TR-1180T, National Aerospace Laboratory, Tokyo, Japan, Oct. 1992.

[18]Traub, L. W., "Effects of Delta Planform Tip Sails on the Performance of a Blunt Edged Rectangular Wing," *Aeronautical Journal*, Vol. 101, No. 2, 1997, pp. 87–92.

[19]Francis, M. S., and Kennedy, D. A., "Formation of a Trailing Vortex," *Journal of Aircraft*, Vol. 16, No. 3, 1979, pp. 148–154.

[20]Traub, L. W., "Simple Prediction Method for Location of Vortex Breakdown on Delta Wings," *Journal of Aircraft*, Vol. 33, No. 2, 1996, pp. 452–454.